AIAA Aviation
22-26 June 2015, Dallas, TX
21st AIAA/CEAS Aeroacoustics Conference

Bio-Inspired Trailing Edge Noise Control

Ian A. Clark[1], W. Nathan Alexander[2] and William Devenport[3]
Center for Renewable Energy and Aerodynamic Testing,
Virginia Polytechnic Institute and State University, Blacksburg, Virginia 24060

Stewart Glegg[4]
Florida Atlantic University, Boca Raton, Florida 33431

Justin W. Jaworski[5]
Lehigh University, Bethlehem, Pennsylvania 18015

Conor Daly[6] and Nigel Peake[7]
University of Cambridge, Cambridge CB3 0WA, UK

Strategies for trailing edge noise control have been inspired by the downy canopy that covers the surface of exposed flight feathers of many owl species. Previous wind tunnel measurements have shown that canopies of similar characteristics can reduce surface pressure fluctuations on the underlying surface by as much as 30dB, and significantly attenuate roughness noise generated by that surface. In the present work, surface treatments have been designed to replicate the effects of the canopy in a form suitable for application to an airfoil. The treatments were installed directly upstream of the trailing edge to modify the boundary layer turbulence prior to acoustic scattering by the edge. Over 20 variants of these designs have been tested by performing aeroacoustic wind tunnel measurements on a tripped DU96-W180 airfoil at chord Reynolds numbers up to 3 million. Compared to the unmodified airfoil, the treatments were found to be effective, providing up to 10dB of broadband attenuation of trailing edge noise. The treatment remains effective throughout a wide parameter range and is not highly dependent on a particular geometry, but there appears to be strong potential for optimization. Treatments were found to be effective over an angle of attack range that extends over 9 degrees from zero lift. Aerodynamic impact of the treatment appears minimal.

I. Introduction

This paper describes an experimental study aimed at trailing edge noise control strategies inspired by the unique features found on the wings of owls that use acoustic stealth while hunting prey (Graham, 1934). These features include a comb of evenly-spaced bristles along the wing leading-edge, investigated by Kroeger *et al.* (1972), a porous and elastic trailing edge fringe, and fine downy hairs that coat the exposed surfaces of the flight feathers. Jaworski and Peake (2013a, 2013b) analyzed the trailing edge condition and found that both porosity and flexibility weaken the well-known fifth-power dependency of the radiated acoustics of a trailing edge, with the greatest reduction in edge amplification occurring when these characteristics are combined. Our concern here is over noise control strategies inspired by the downy hairs.

The work described in this paper follows on from the study of Clark *et al.* (2014). Their interest was in the potential of a hairy surface to suppress noise generated by roughness lying underneath. They showed that the hairs grow nearly perpendicular out of the feather surface, but then lean over to form a canopy suspended about 0.5-mm above the feather substrate, with an open area ratio of about 70% (figure 1). Wall-jet wind tunnel experiments were performed to examine the aeroacoustic effects of artificial canopies designed to mimic the effects of a canopy of this type on the surface pressure fluctuations and roughness noise generated by an underlying rough surface. Efforts included shrouding surfaces using canopies constructed from materials of the type used for wedding veils (figure 2a)

[1] Graduate Student, Department of Aerospace and Ocean Engineering, Student Member AIAA
[2] Research Assistant Professor, Department of Aerospace and Ocean Engineering, AIAA Member.
[3] Professor, Department of Aerospace and Ocean Engineering, Associate Fellow AIAA.
[4] Professor, Department of Ocean and Mechanical Engineering, Associate Fellow AIAA.
[5] Assistant Professor, Department of Mechanical Engineering and Mechanics, Senior Member AIAA.
[6] Postdoctoral Scholar, Department of Applied Mathematics and Theoretical Physics.
[7] Professor, Department of Applied Mathematics and Theoretical Physics, Member AIAA.

Figure 1. *Close-up view of a flight feather of a Great Grey Owl showing the canopy structure formed by the hairs*

and a series of canopies constructed using large numbers of parallel fibers, oriented in the flow direction just above the flow surface (figure 2b).

Measurements of surface pressure fluctuations underneath these canopies and of the roughness noise generated by surfaces shrouded by these canopies produced some surprising results. Even though the canopies had high open area ratios of about 70% they attenuated surface pressure fluctuations underneath them by as much as 30dB. The canopies were also found to attenuate broadband roughness noise, presumably because the acoustic source for roughness noise is the surface pressure fluctuation (Glegg and Devenport, 2009).

These unexpected findings spawned a whole new line of inquiry when it was realized that such a large reduction in surface pressure fluctuations might also serve to greatly attenuate trailing edge noise if a treatment replicating the effects of the canopy could be designed that was suitable for application to an airfoil. This paper describes an experimental study of a series of treatments inspired by this idea. An extensive series of wind tunnel tests have been performed on a wind turbine airfoil at near full scale Reynolds number. Measurements of the sound radiated by the airfoil trailing edge have been made both for the clean airfoil and with an extensive series of trailing edge treatments inspired by the owl down and the results of Clark *et al.* (2014). The effects of a broad range of treatment parameters were studied. We find that the treatment produces a broadband reduction in trailing edge noise levels of up to 10dB. The treatment remains surprisingly effective throughout a wide parameter range and is not highly dependent on a particular geometry, but there appears to be strong potential for optimization. The treatment is effective over an angle of attack range that extends to over 9 degrees from the zero lift condition.

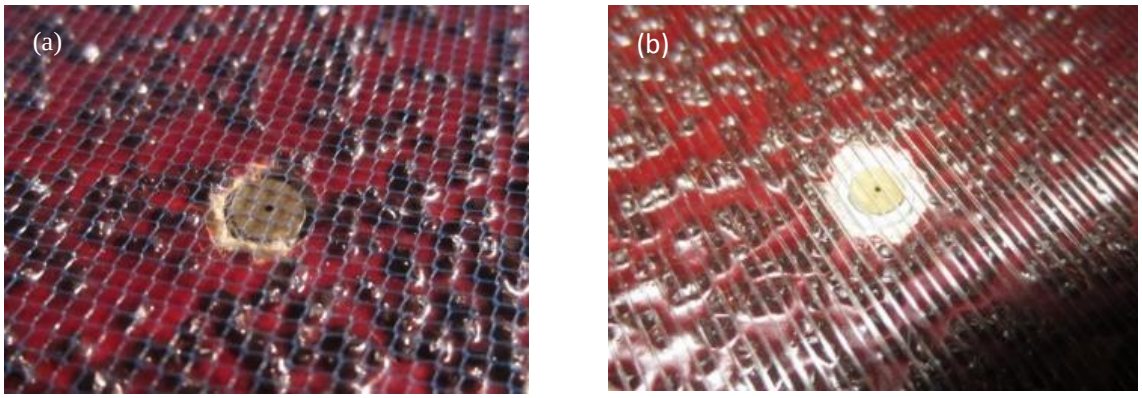

Figure 2. *Example fabric canopy arrangements studied in the wind tunnel, shown shrouding a sandpaper type rough surface. (a) Commercial wedding-veil type fabric with multi-directional fibers. (b) Custom designed unidirectional fiber fabric with fibers oriented only in the flow direction*

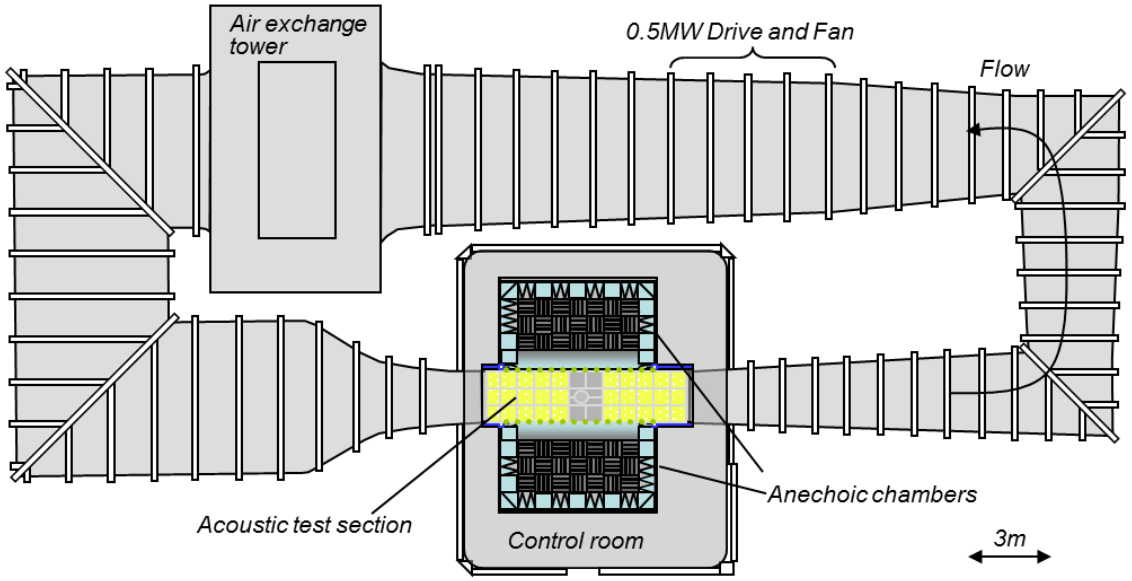

Figure 3 *Plan view schematic of the Virginia Tech Stability Wind Tunnel in anechoic configuration*

II. Apparatus and Instrumentation

A. Stability Wind Tunnel

All tests were performed in the Virginia Tech Stability Wind Tunnel. This facility is a continuous, single return, subsonic wind tunnel with 7.3-m long removable rectangular test sections of square cross section 1.85m on edge. The general layout is illustrated in Figure 3.

The tunnel is powered by a 0.45-MW variable speed DC motor driving a 4.3-m propeller that provides a maximum speed in the test section (with no blockage) of about 80m/s. Ahead of the test section, flow is directed into a 5.5×5.5m settling chamber containing 7 turbulence-reducing screens each with an open area ratio of 0.6 and separated by 0.15m. Flow exits this chamber through the 9:1 contraction nozzle which further reduces turbulence levels and accelerates the flow to test speed as it enters the test section (figure 4).

Flow through the empty test section is both closely uniform and of very low turbulence intensity. Table 1 shows measurements from 2006 of free stream turbulence levels as a function of flow speed. Turbulence levels are as low 0.016% at 12m/s and increase gradually with flow speed. Choi and Simpson (1987) measured the lateral integral scales of the streamwise velocity in both the horizontal L_z and vertical L_y directions. They found L_z=56mm for 15m/s and 28mm for 37.5m/s and L_y=122mm for 15m/s and 25mm for 37.5m/s.

The Stability Wind Tunnel aeroacoustic test section was used for the present study, figures 4 and 5. This has acoustically treated lower and upper walls, consisting primarily of Kevlar-covered metal perforate panels backed by 0.45m sound absorbing foam wedges. The central 4.2-m length of both side walls are made from Kevlar panels placed under tension. The Kevlar contains the vast bulk of the flow, and is almost transparent to sound (see Devenport *et al.*, 2013). Sound generate by a model placed at the center of the test section can therefore propagate out of the flow and into anechoic chambers placed on either side of the test section. The chambers, lined with 0.61-m foam wedges, are anechoic down to 190Hz. The 4.2-m long, 2.6-m deep and 3-m high interior volume of the chambers allows for the placement of acoustic instrumentation. This unusual arrangement has a number of advantages over a conventional free-jet tunnel. It eliminates the need for a jet catcher, reduces aerodynamic interference corrections by about a factor of 4, allows for a long test section that provides a clear separation between model generated sound and the parasitic noise of the facility, and permits acoustic instrumentation to be placed close to the model, yet out of the flow. Further details of the facility and its calibration are given by Devenport *et al.* (2013). Acoustic and

Freestream Velocity	RMS Streamwise Fluctuations
U_∞ (m/s)	u'/ U_∞
12	0.016%
21	0.021%
30	0.024%
48	0.029%
57	0.031%

Table 1. Freestream Turbulence Levels

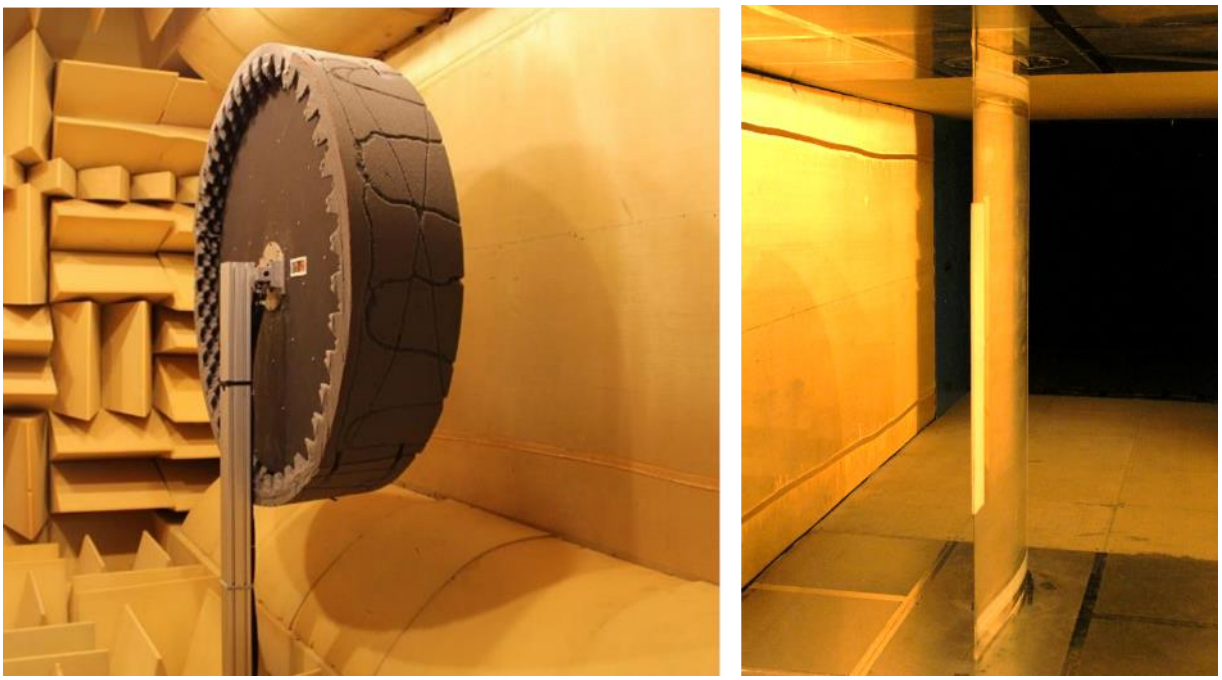

Figure 4. *Views of the 0.8-m chord DU96-W180 airfoil mounted in the anechoic test section (right) and of the 117-microphone phased array system installed in the port-side anechoic chamber directed at the suction side of the airfoil (left).*

aerodynamic corrections applied to measurements made in this test section are also described by Devenport *et al.* (2013).

B. Airfoil model, tripping, lift measurement

The 0.8-m chord airfoil model used for the experiments is illustrated in figure 4, as installed in the test section. The model has a DU96-W180 section – a standard wind turbine blade profile with a maximum thickness of 18% chord. The model was assembled from 0.05-m thick laminates, each cut with the airfoil profile. The laminate construction allows for easy installation of internal instrumentation, while careful alignment and accurate machining of the laminates ensures a smooth and continuous airfoil surface.

0.5-mm high serrated tape (Glasfaser-Flugzeug-Service GmbH 3D Turbulator Tape) was used to trip the airfoil boundary layers. The tape was applied at the 5% and 10% chord locations of the suction and pressure sides of the airfoil, respectively.

Pressure distributions and lift on the model were measured using some 80 1mm pressure taps distributed around the profile. Pressures were sensed using Esterline 9816/98RK pressure scanners with a range of ±2.5psi (rated accuracy of ±0.05% full scale) connected to the pressure taps through 1.6-mm Tygon tubing.

C. Measurement of drag and reference conditions

Tunnel free-stream velocity was monitored using the pressure difference between static taps located in the walls of the wind tunnel settling chamber and contraction, sensed using the Esterline 9816/98RK pressure scanner system. Temperature in the test section was monitored using an Omega Thermistor type 44004 (accuracy ±0.2°C) and the ambient absolute pressure was determined using a Validyne DB-99 Digital Barometer (resolution 0.01" Hg).

For some conditions a rake of Pitot and static probes was used to measure profiles through the airfoil wakes and infer the drag using a momentum balance approach. The rake consists of 113 1.6-mm diameter Pitot probes and 7 Pitot-static probes distributed over a 1.8-m length. Mounted on the rake system are four DTC Initium ESP-32HD 32-channel pressure scanners with a range of ±2.5psi to which the tubes are connected. The rake is acoustically noisy and so was not used during acoustic measurements.

D. Sound measurement

Airfoil trailing edge noise was measured using a phased array system located in the port-side anechoic chamber facing the suction side of the airfoil, figure 4. The array has 117 Panasonic electret microphones type WM-64PNT

arranged in 9 spiral arms mounted on a solid 1.1 m diameter carbon-fiber disk. These microphones have a flat frequency response from 20-16000Hz. The array was calibrated to within +/-5° phase and 0.4 dB amplitude from 500Hz to 16000Hz. The array was mounted in the port side chamber which was the suction side of the airfoil slightly upstream of the ¼ chord position. Boundary layer refraction effects, convective effects, pressure doubling due to the microphones being mounted on a solid surface, and attenuation through the Kevlar cloth have all been accounted for in post-processing. Data were recorded simultaneously at 51200Hz for 32 seconds with two 64 channel PCI-based data acquisition cards. The signals were processed through an anti-aliasing filter at 20kHz. Spectral quantities were computed by averaging the Fourier transform of blocks of 8192 samples. The diagonal of the cross-spectrum was removed in order to omit uncorrelated noise in the beamformed maps. Integrated spectra were computed by integrating the beamformed results over a selected region.

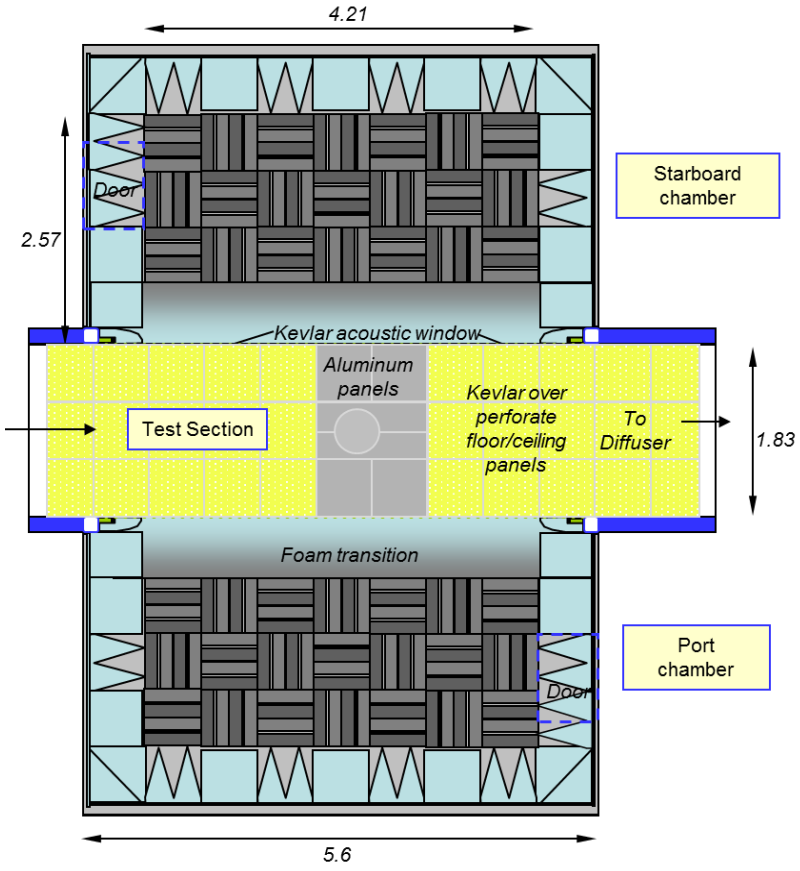

Figure 5. *Plan view cross-section of the anechoic system as installed showing the test section flanked by the two anechoic chambers. Dimensions in meters.*

E. Trailing edge noise treatments

Two different treatment designs were developed with the goal of replicating the effects of a canopy on reducing surface pressure fluctuations, seen in the

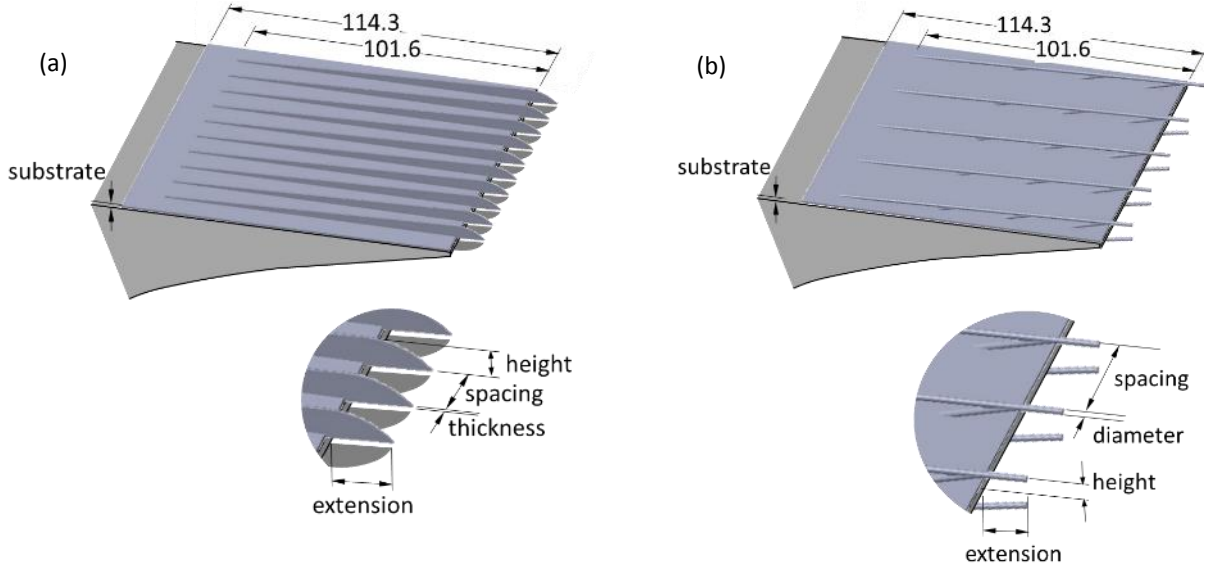

Figure 6. *Treatment designs tested on the DU96-W180, (a) finlet fence, (b) finlet rail. Diagrams show finlets attached to the trailing edge portion of the airfoil, dimensions in millimeters.*

wall-jet tunnel, in a form suitable for application to an airfoil in external flow. The designs are illustrated in figure 6 and are referred to as finlet fences and finlet rails. A total of 20 variants on these designs were fabricated using rapid prototyping and tested. All involved the rail or fence treatment beginning 101.6-mm upstream of the trailing edge (87.3% chord), and in all cases the treatment was supported on a thin sheet of material (the substrate) glued to the airfoil, with its leading edge placed 114.3-mm upstream of the airfoil trailing edge (85.7% chord). Only the middle half span of the airfoil was treated (see figure 4). The leading edge of the substrate was, in all cases, faired to the airfoil surface by covering it with 0.1mm thick metal tape.

The upper edges of finlet fences (figure 6a) are designed to present the same geometry to the airfoil boundary layer flow as the unidirectional canopy of figure 2b. A total of 14 such fence configurations were tested, including variations in finlet spacing, height, thickness, extension past the trailing edge, and substrate thickness. The rails (figure 6b) more explicitly replicate the fiber geometry of the canopy in figure 2b, with streamwise cylindrical elements mounted from the surface using periodic swept supports. A total of 6 such configurations were tested. Table 2 shows the full test matrix for both types of configurations. The table also includes the control cases, including the untreated tripped airfoil and two cases in which only substrate layers were applied to the airfoil surfaces.

Config. No.	Height	Spacing	Thickness/Rail Diameter	TE extension	Substrate	Suction only	C_p/lift	Drag	Acoustics
CONTROL CASES									
0	-	-	-	-	-	-	Y	Y	Y
2	-	-	-	-	0.5	-	Y	Y	Y
10	-	-	-	-	0.75	-	Y	-	Y
FENCE CASES									
3	4	1	0.5	10	0.5	-	Y	-	Y
1	4	1	0.5	0	0.5	-	Y	-	Y
5	4	4	0.5	10	0.5	-	Y	-	Y
13	4	6	0.5	10	0.75	-	Y	-	Y
7	4	10	0.5	10	0.5	-	Y	-	Y
11	2	1	0.5	10	0.75	-	Y	-	Y
6[1]	4	1	0.5	10	0.5	-	Y	-	Y
12[2]	4	1	0.5	10	0.75	-	Y	-	Y
8	8	4	0.5	10	0.5	-	Y	Y	Y
9	4	4	2	10	0.75	-	Y	-	Y
1S	4	1	0.5	0	0.5	Y	Y	-	Y
3S	4	1	0.5	10	0.5	Y	Y	-	Y
8S	8	4	0.5	10	0.5	Y	Y	-	Y
26S	16	4	0.5	0	0.5	Y	Y	-	Y
RAIL CASES									
14	4	2.5	1.25	10	0.75		Y	-	Y
15	4	2.5	1.25	0	0.75	-	Y	-	Y
17	8	2.5	1.25	10	0.75	-	Y	-	Y
18	4	5	2.5	10	0.75	-	Y	-	Y
20	8	10	1.25	10	0.75	-	Y	-	Y
19[1]	4	2.5	1.25	10	0.75	-	Y	-	Y

Table 2. List of finlet cases and measurements made. Dimensions are in millimeters

III. Results and Discussion

Measurements were made at 50 and 60m/s corresponding to chord Reynolds numbers of 2.5 and 3.0 million respectively. We present here only results for 3.0 million since those measured at 2.5 million are almost identical. For all cases the airfoil boundary layers were fully turbulent, having been tripped as described in section II.B. For all conditions, table 2, far-field sound and surface pressure (and therefore lift) measurements were made with the airfoil pitched from -4 to 16 degrees angle of attack in approximately two degree increments. This range encompasses zero lift ($\alpha \approx -2.5°$) as well as stall ($\alpha \approx 11°$). In all cases, a measurement sequence with a treated condition was immediately followed or preceded by a measurement of the untreated condition, so as to minimize the experimental uncertainty between the two and establish (by comparing the many untreated-condition measurements) the repeatability of the results. Thus the wind tunnel entry included many repeat measurements of configuration 0, which will be referred to as the 'clean condition'. Configuration 8 was also repeated so that drag measurements could be made with the rake system without interference of the acoustic measurement.

[1] Fence/rail length upstream of the trailing edge varied periodically in the spanwise direction with one period being the sequence 101.6mm, 12.7mm, 25.4mm, 12.7mm, 50.8mm, 12.7mm, 25.4mm and 12.7mm.

[2] Fence length upstream of the trailing edge varied periodically as in configuration 6, but with fence height scaled to 4mm, 2.5mm, 3mm, 2.5mm, 3.5mm, 2.5mm, 3mm, and 2.5mm in the same periodic sequence, respectively.

A. Noise measurements made with the clean airfoil

Figures 7 and 8 summarize the trailing edge noise measurements made with the clean airfoil at Re = 3 million. Figure 7 shows sample beamform maps at 3kHz. All spectra are shown on the same dB scale with a 10dB range, but the overall dB reference is arbitrary. Figure 7 compares farfield spectra integrated over the central 25% of the blade span, as indicated by the dashed box shown in figure 7(a). Starting at the zero lift angle of attack (figure 7a) the trailing edge noise is clearly detectable at this frequency and is seen to form a clean uniform band along the trailing edge. As the angle of attack is increased the trailing edge noise actually decreases slowly (note the change in the absolute level of the color scales in figure 7) so that, once the quietest angle of attack of 3 degrees is reached, the spurious lobes associated with the background noise levels generated by the facility appear more prominent. The trailing edge noise is still easily distinguished, however, and remains so through 6.9 degrees angle of attack until the airfoil stalls. At stall, airfoil generated noise levels greatly increase (e.g. figure 7e) and a stall pattern with two spanwise cells is formed, clearly visible in the beamform map.

One 12th octave band integrated spectral levels for angles of attack of -2.5, -0.5, 3 and 6.9 degrees are compared in figure 7. The area of integration for this and subsequent similar figures is shown by the black box drawn on figure 7(a). The difference in trailing edge noise levels for varying angles of attack only becomes distinguishable above about 1500Hz. This may be partly due to the spot-size of the phased array which becomes comparable to the integration area at this frequency. Above 1500Hz the sound spectra are seen will be discussed

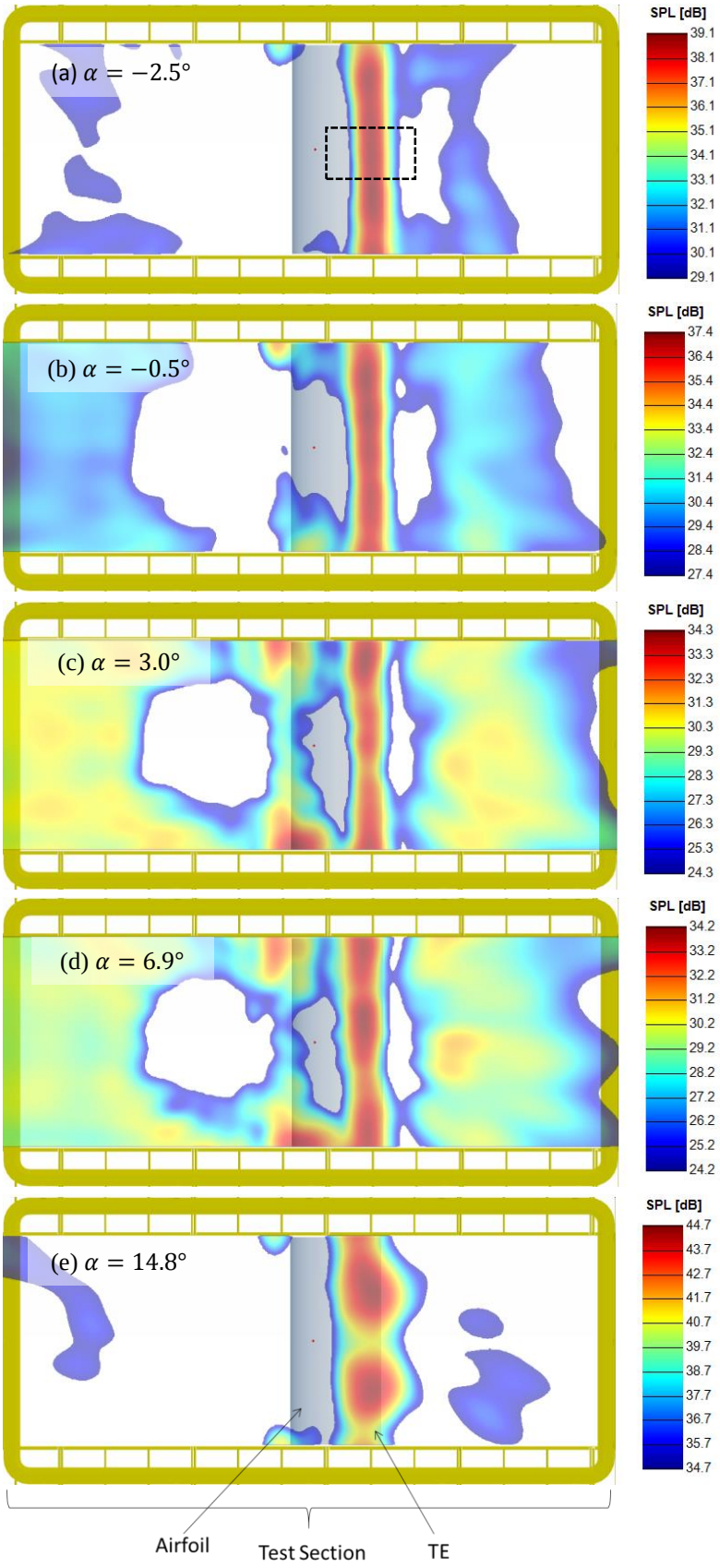

Figure 7. *Beamform maps showing the trailing edge noise radiated by the untreated DU96-W180 at 3kHz as a function of angle of attack. Re=3 million.*

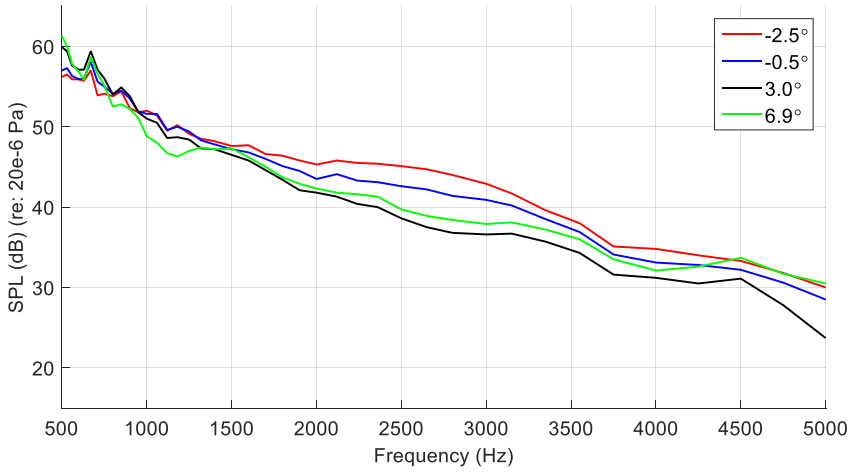

***Figure 8**. Noise spectra for the untreated DU96-W180 at Re=3 million, as a function of angle of attack, obtained by integrating phased array results over the central 25% of the airfoil span, as indicated by the dashed region in figure 6a.*

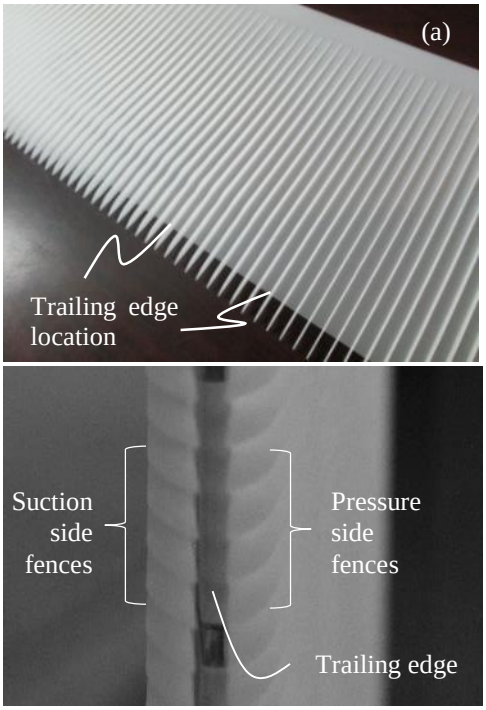

***Figure 9**. Configuration 5. (a) Before attachment to the airfoil. (b) After attachment to both sides of the airfoil (view seen looking upstream at the trailing edge). Note the gap between the fence extensions on either side of the trailing edge.*

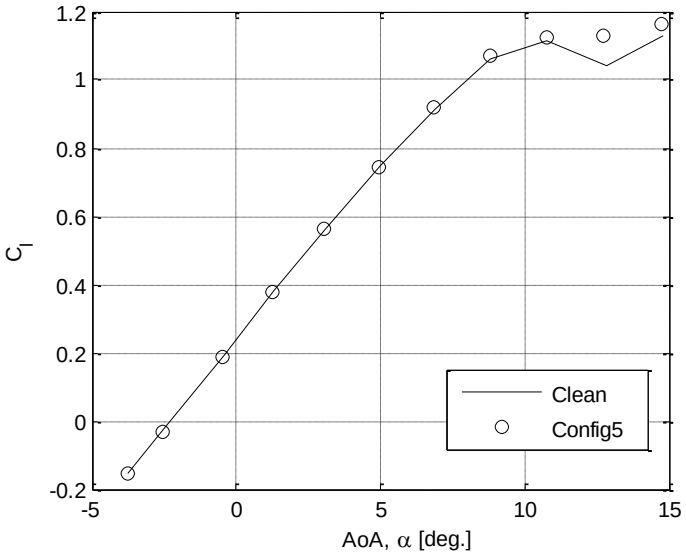

***Figure 10**. Lift coefficient plotted against angle of attack for the untreated ('Clean') and baseline treated ('Config 5') DU96-W180 at Re=3 million.*

further below, this may to be broadband in all cases. The sound level variations with angle of attack observed at 3kHz in the beamform maps are seen to be representative of the whole frequency range, with spectral levels lowest at 3 degrees angle of attack where they are up to 7dB lower than those seen at zero lift.

B. Effects of the baseline fence treatment

We examine first the effects of the baseline airfoil treatment, which we take as configuration 5. The treatment, shown in figure 9, consists of 0.5-mm thick fences with a maximum height of 4mm spaced every 4mm across the span. The fences extend by 10-mm past the trailing edge and are attached to the airfoil via a 0.5-mm thick substrate. The treatment was placed on both sides of the airfoil and covered the center half-span of the model, so that direct comparisons could be drawn with the untreated regions at the ends of the airfoil. Figure 10 shows measurements of the lift on the airfoil as a function of angle of attack. There appear to be no detrimental effects of the treatment on the lift and, indeed, it appears that the lift is slightly enhanced post stall. Note that lift measurements were integrated using pressure distributions measured over the first 85% of the airfoil chord, extrapolated to the trailing edge, since the last 15% of the chord was covered by the treatments when they were applied. Checks run with the clean airfoil showed that neglecting the data in this region had no significant effect on the integrated lift.

Figure 11 shows beamform maps for the treated airfoil at Re=3 million for the unstalled angles of attack (the treatment had no discernable influence on the airfoil sound, either positive of negative, post stall). Integrated spectra for the treated and untreated airfoil are compared for the zero lift angle of attack in figure 12, and for other sample angles of attack in figure 13. At the zero lift angle of attack (figure 11a) the beamform map shows no discernable trailing edge noise coming from the treated portion of the airfoil, whereas the untreated portions appear almost unaltered from the results shown in figure 7(a). This indicates about a 10dB attenuation at 3kHz for this condition. As the angle of attack increases (figures 11(b) through (d)) the effectiveness of the treatment diminishes but is still substantial at -0.5 and 3 degrees angle of attack and is certainly still detectable at 8 degrees.

Figure 12 shows the effectiveness of the treatment over a broader range of frequencies at the zero lift condition ($\alpha = -2.5°$). The attenuation achieved

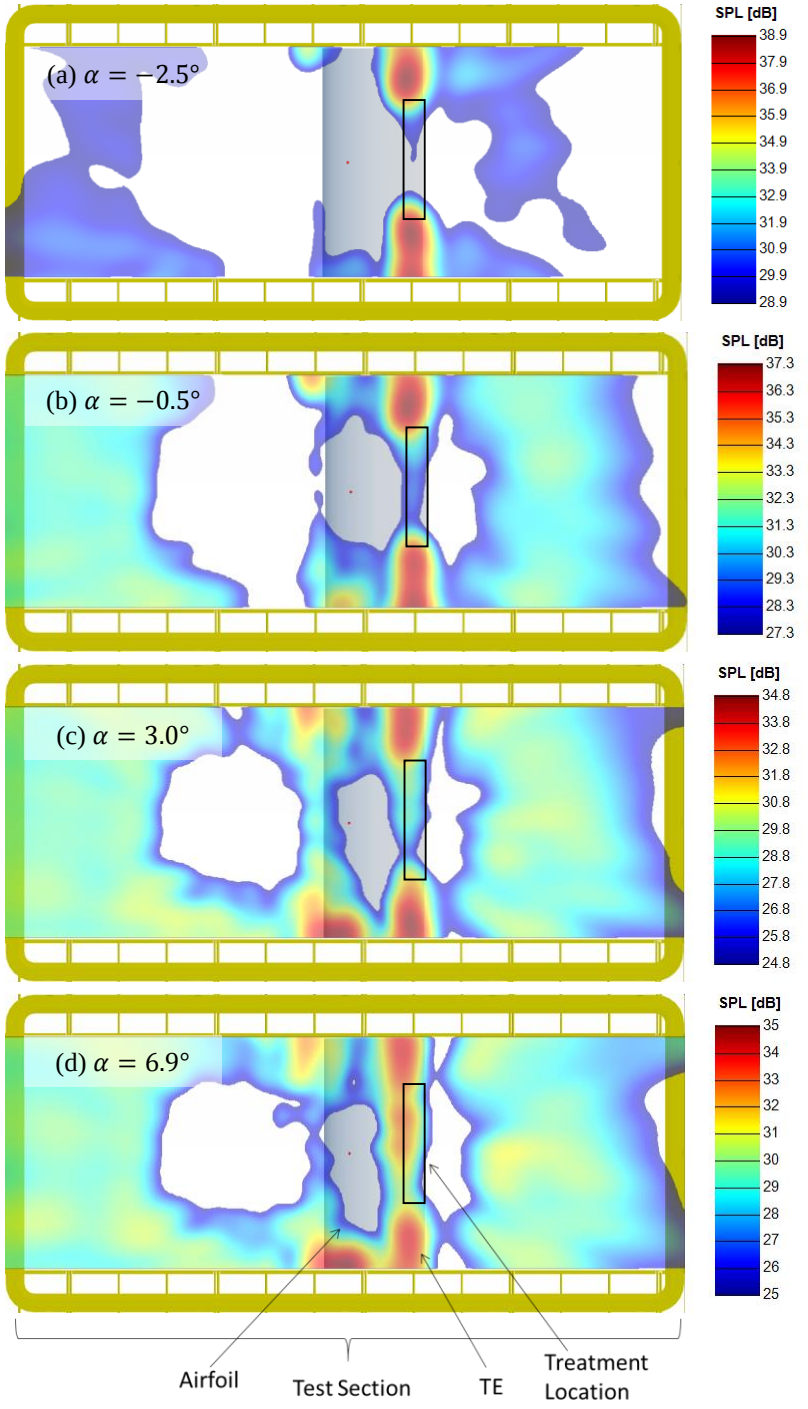

Figure 11. *Beamform maps showing the trailing edge noise radiated by the DU96-W180 at 3kHz as a function of angle of attack with the baseline (configuration 5) treatment applied across the central half span (as indicated by the black square). Re=3 million.*

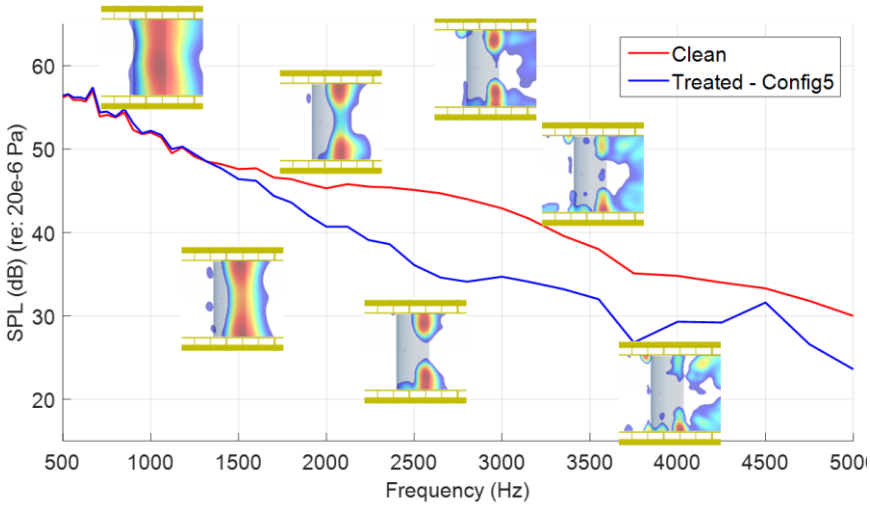

***Figure 12**. Noise spectra for configuration 5 treatment compared to results for the clean case. Re=3 million, -2.5 degrees angle of attack. Inset images show beamform maps of the treated airfoil noise to illustrate the blurring effects of the large spot size at frequencies below about 2kHz.*

by the treatment is clearly broadband with reductions between 5 and 10dB for frequencies between 2kHz and 5kHz. For frequencies below 2kHz, the effectiveness of the treatment appears to diminish, ultimately disappearing at about 1400Hz. However, this is at least partly an artificial effect of the diminishing ability of the array to focus as the frequency is reduced. To illustrate this, figure 12 includes thumbnail images showing beamform maps of the treated airfoil sound field at different frequencies. Each thumbnail has been centered on the frequency to which it refers. At about 1500Hz the spot size of the array has become comparable to the width of the treated portion of the airfoil span and the lobes associated with the untreated portions at the two ends of the airfoil have begun to merge. There still appears to be some attenuation of the sound between the untreated regions but it is largely obscured by this blurring. As the frequency is reduced to 1kHz, the ability of the array to distinguish features on the scale of the treated portion of the span has been completely lost. Understanding the low-frequency performance of the treatment will therefore have to await further experiments.

The broadband effectiveness of the treatment is illustrated for all the sample angles of attack in figure 13. At -0.5 degrees angle of attack the attenuation achieved with the treatment above 2kHz is between about 3 and 7dB. At 3 degrees, the effectiveness of the treatment is somewhat diminished at frequencies below about 3.5kHz, but is enhanced at higher frequencies, reaching about 12dB near 4kHz. At 6.9 degrees angle of attack the effectiveness of the treatment is noticeably reduced, but significant reductions in sound, of up to about 3dB, are still visible at frequencies over 2.5kHz. At no angle of attack is the treatment seen to have any detrimental effect on the radiated sound.

It is important to recognize that the substrate is not an inactive component of the treatment. Figure 14 shows the effect on integrated acoustic levels of adding only a 0.5 and a 0.75-mm thick substrate to the airfoil, as compared to the clean case. (Note that configuration 5 is mounted on the thin, 0.5-mm substrate.) At α =-2.5º and -0.5º the substrate adds to the trailing edge noise at around 1500Hz and 1800Hz for the 0.75-mm and 0.5-mm thicknesses respectively, quite possibly because of vortex shedding enhanced because of the substrate adding to the trailing edge thickness. At the same time, sound levels with the substrates are somewhat lower (by up to 5dB for the 0.5-mm and 7dB for the 0.75-mm) at higher frequencies. This could be because of a non-linear re-distribution of energy into the lower-frequency vortex shedding motions. At $\alpha = 3^{o}$ and 6.9º the increased levels ascribed to vortex shedding are smaller or absent. At the same time the noise reductions are also smaller and don't appear until higher frequencies.

At the very least, the fences are clearly suppressing the detrimental effects of the substrate at low frequencies while enhancing the noise reduction at high frequencies. One possible explanation is that the finlets suppress the surface pressure fluctuations at the airfoil trailing edge, and also coherent vortex shedding here by breaking up the spanwise correlation lengthscale of the boundary layer. One can imagine the unidirectional canopy of Clark *et al.* (2014) reducing wall pressure fluctuations by a similar mechanism.

C. Effects of the fence parameters

In this section we examine the effects of varying the fence parameters. Note that all the treated cases produced lift characteristics almost identical to those of configuration 5, i.e. the same as, or slightly better than, the untreated airfoil. Figure 15 shows the effects of changing the fence spacing by comparing integrated sound levels from configurations 3, 5, 13 and 7 representing spacings of 1, 4, 6 and 10mm. Photographs showing three of these four treatments are shown in figure 16.

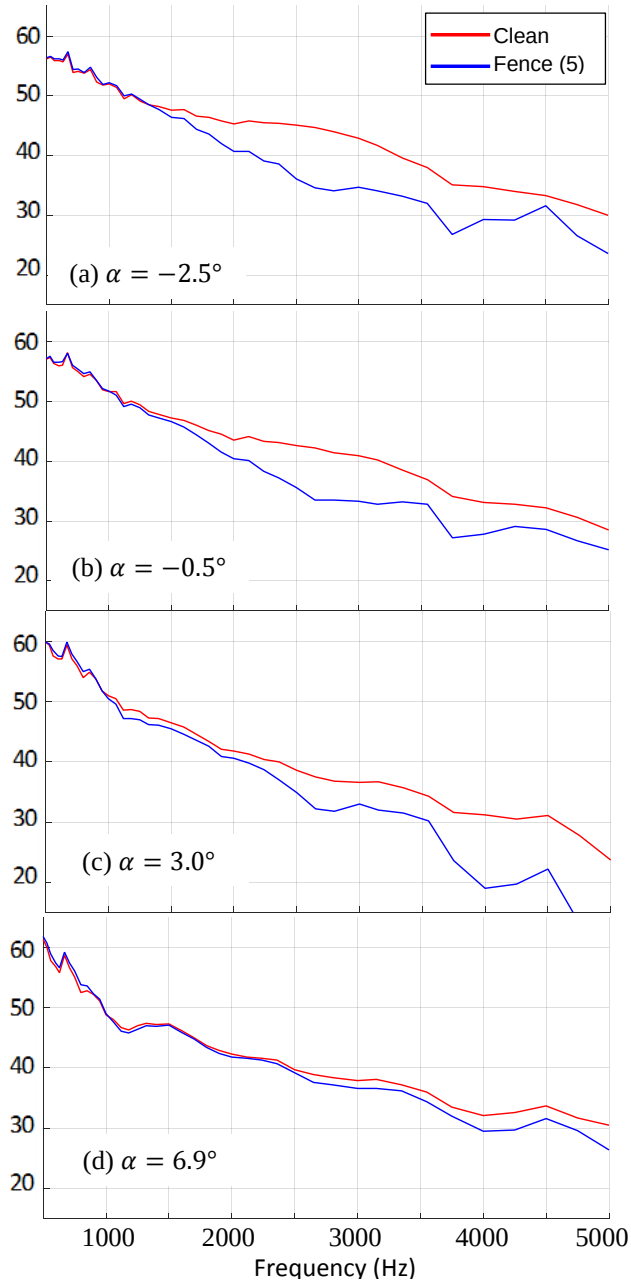

Figure 13. *Noise spectra (in SPL re* $20\,\mu Pa$*) for configuration 5 treatment compared to results for the clean case. Re=3 million.*

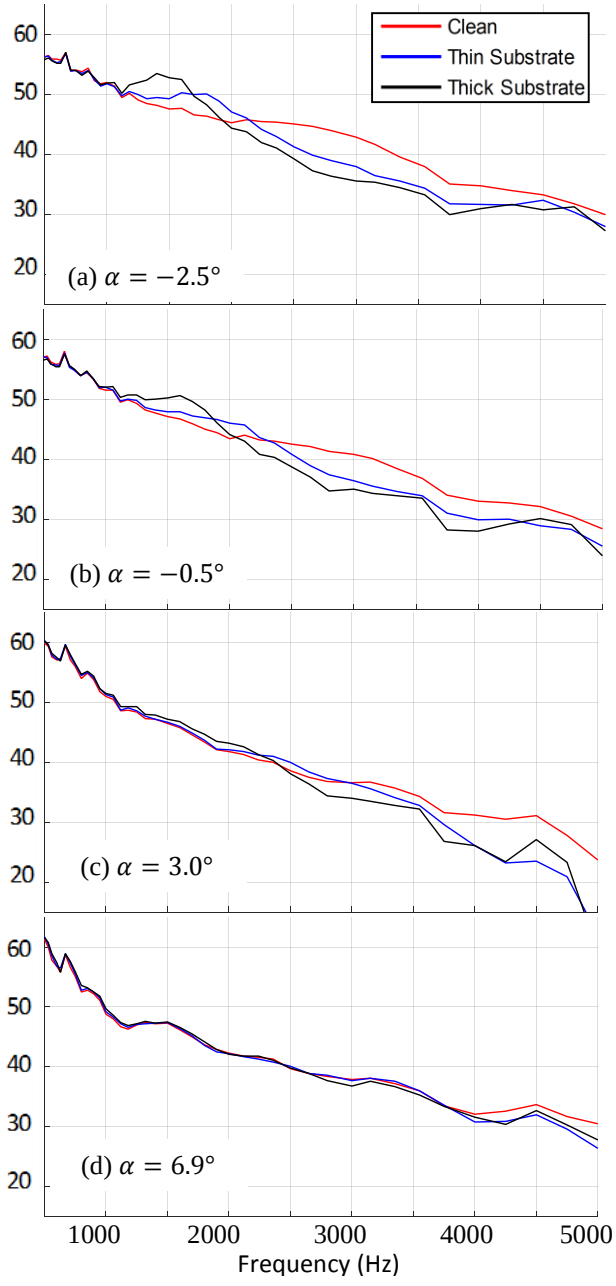

Figure 14. *Noise spectra (in SPL re* $20\,\mu Pa$*) for configurations 2 and 10 showing substrate alone effects compared to the clean case. Re=3 million.*

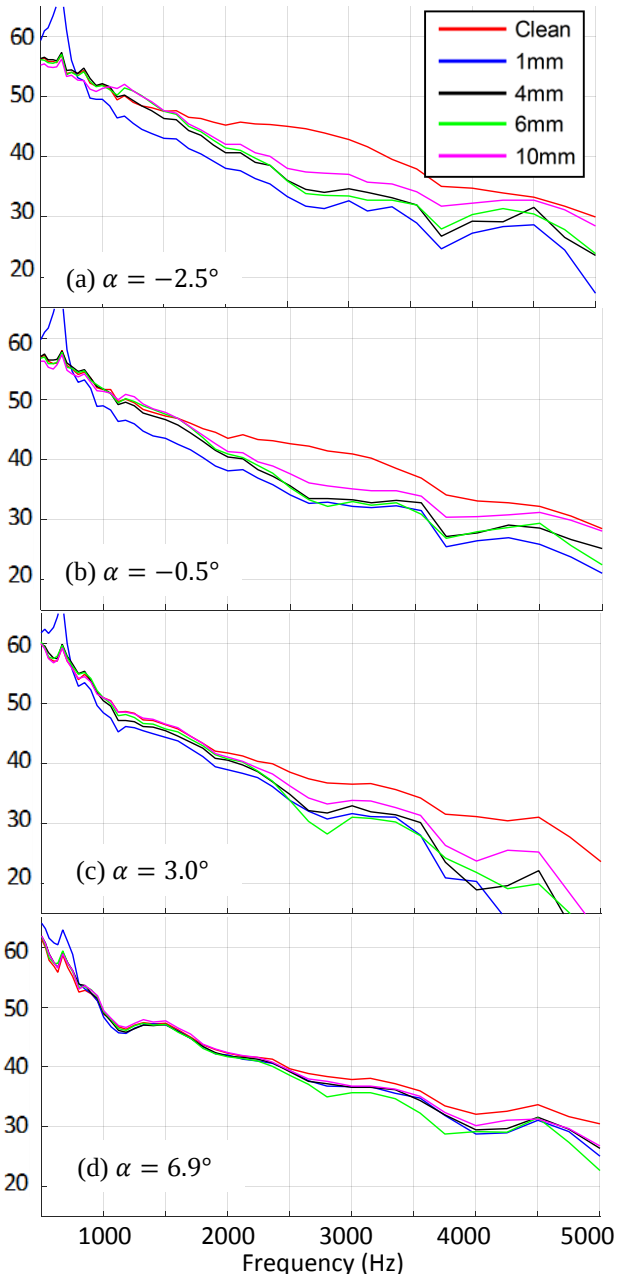

***Figure 15**. Noise spectra (in SPL re 20 μPa) for configurations 3, 5, 13 and 7 showing the effects of fence spacing on noise radiation compared to the clean case. Re=3 million.*

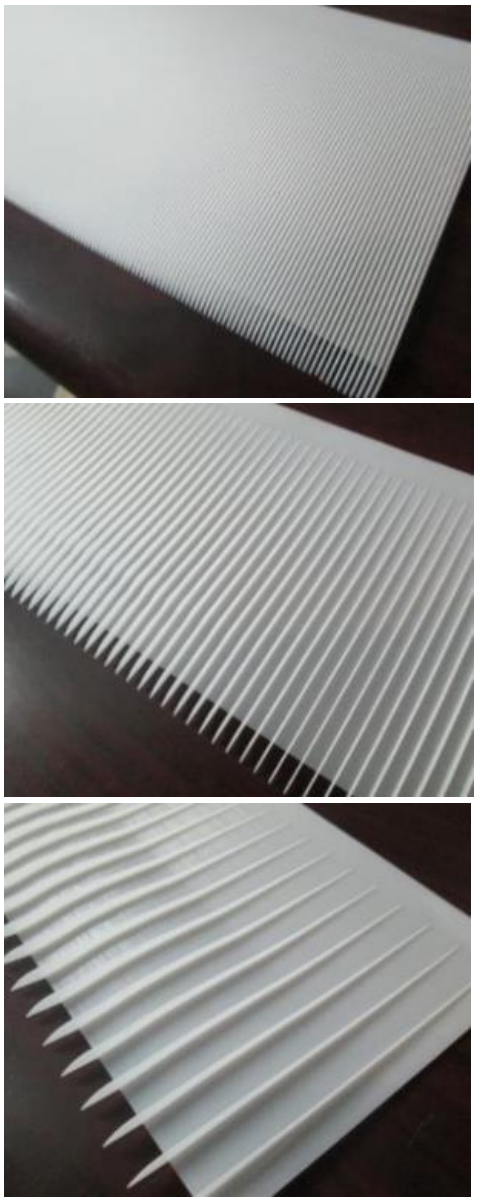

***Figure 16**. Photographs of treatments 3, 5 and 7, fence treatments with 1mm, 4mm and 10mm spacing respectively, before application to the airfoil*

Overall, the noise spectra appear to show a clear progression with fence spacing for angles of attack α = -2.5º, -0.5º and 3º. At these conditions, the 6-mm spacing produces quite similar noise reductions to the 4-mm described above. Reductions with the 10-mm spacing are less, particularly at frequencies over 3.5kHz. Reductions with the 1mm are greater, by 1-4dB over almost all the frequency range. This dependence appears consistent with the fences limiting the spanwise correlation length scale – the smaller the spacing, the smaller the maximum correlation scale that can survive to the trailing edge. There is clearly a limit to the beneficial effect though, in the form of the intense spike that appears in the spectra for the 1-mm spaced fence at around 650Hz. At 60m/s, this frequency corresponds to a distance scale of about 18-mm (at a Strouhal number of 0.2), which is of the same order as the sum of the trailing edge thickness (2.5 mm), both substrate layers (1 mm) and two fence heights (8mm). The implication is that below a certain minimum spacing, somewhere between 1 and 4mm in this case, the fences start to behave like a solid, much thicker, blunt trailing edge. At $\alpha = 6.9°$ the noise reductions are smaller in all cases, and the dependence on fence-spacing less apparent. Acoustic levels at this angle of attack are slightly lower at high frequencies with the 6-mm spaced fence (configuration 13), perhaps because the substrate used with this configuration was slightly thicker than for the other cases in this comparison (0.75 vs 0.5 mm).

The effects of extending the treatment past the trailing edge are examined in figure 17. This compares integrated noise spectra for case 3 (1-mm spaced, 4-mm high fences extending 10mm past the trailing edge) to case 1 (identical geometry but shortened so that the fences end at the trailing edge). At lower angles of attack, α = -2.5º and -0.5º both configurations produce almost identical acoustic results, including the intense vortex shedding peak associated with the 1-mm spacing. The results are also quite similar at 3º and 6.9º angle of attack except that high frequency noise levels (>3kHz) are noticeably lower without the extension. It appears, therefore, that the extension offers little if any benefit and, indeed, comes at a price at higher angles of attack. This implies that the finlets are, as hypothesized, manipulating the boundary layer structure as it reaches the trailing edge, rather than altering the scattering efficiency by reshaping the trailing edge, as is accomplished by a trailing edge serration or comb. This suggests it may be possible to maximize noise attenuation by combining both control strategies.

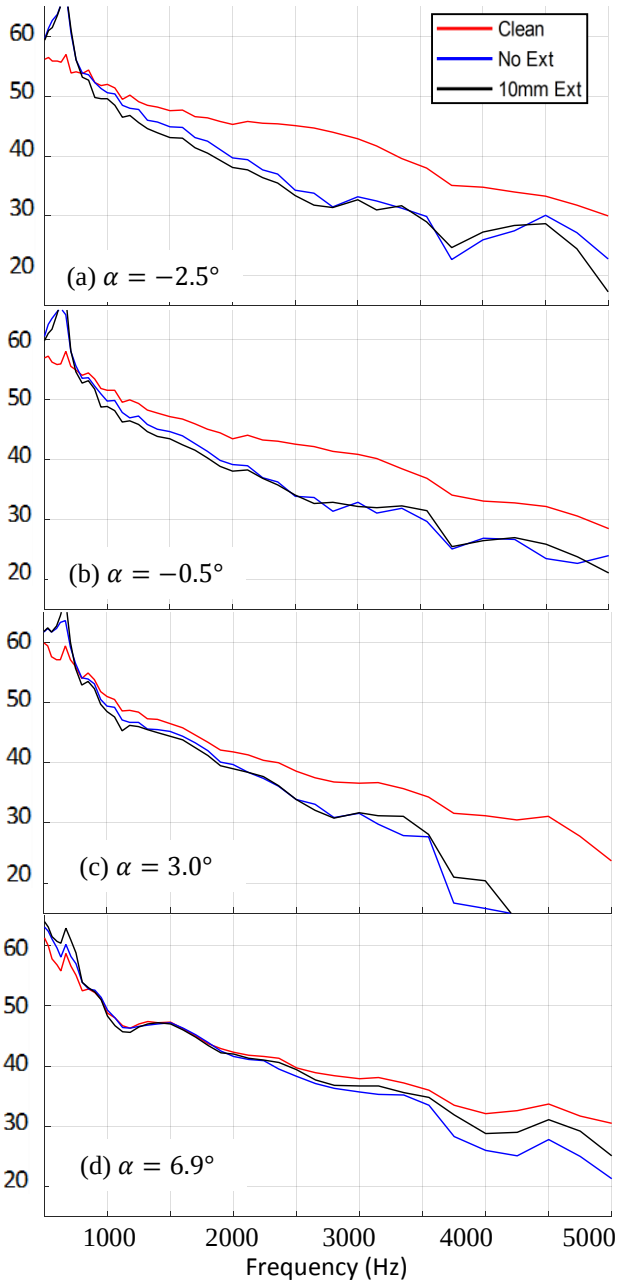

Figure 17*. Noise spectra (in SPL re 20 μPa) for configurations 3 and 1 showing the effects of fence extension over the trailing edge on noise radiation compared to the clean case. Re=3 million.*

Figure 18 examines the effect of fence height on the acoustic signature of the airfoil. Here results for configuration 5 (4mm-high, 4-mm spaced, fences) are compared to those of configuration 8 (8-mm high, 4-mm spaced, fences) and the clean airfoil. At all angles of attack and at almost all frequencies, noise levels are reduced by 1 to 2dB by a doubling of the fence height. This effect can be understood in the context of the boundary layer thickness at the trailing edge. Xfoil calculations suggest displacement thicknesses, for the tripped DU96 at Re=3 million, of 0.9, 1.2, 1.8 and 3.1mm for the suction side and 0.7, 0.5, 0.3, and 0.2mm for the pressure side at α =-2.5º, -0.5º, 3º, and 6.9º respectively.

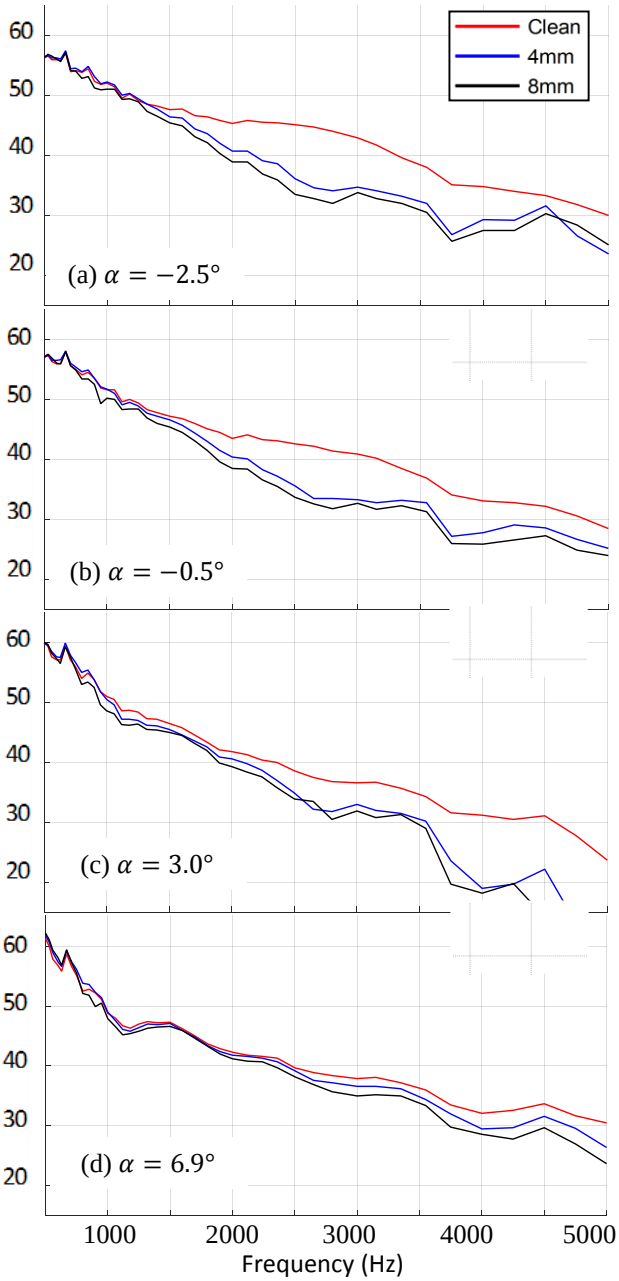

***Figure 18**. Noise spectra (in SPL re 20 μPa) for configurations 5 and 8 showing the effects of fence height on noise radiation compared to the clean case. Re=3 million.*

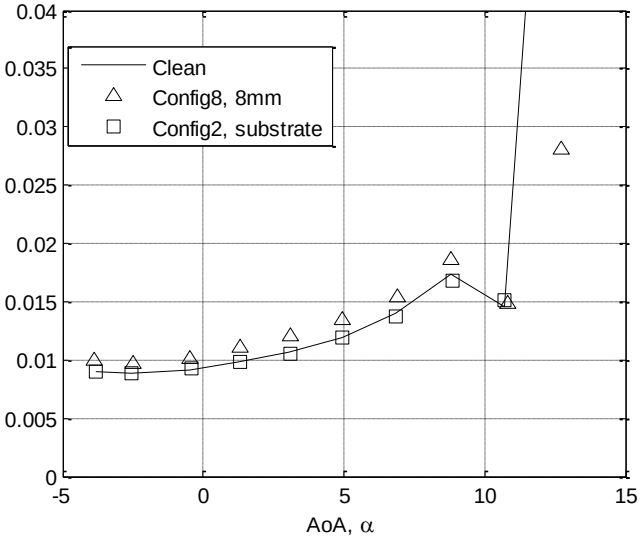

***Figure 19**. Drag coefficient as a function of angle of attack measured for the clean airfoil, with configuration 8, and with the substrate alone. Re=3*

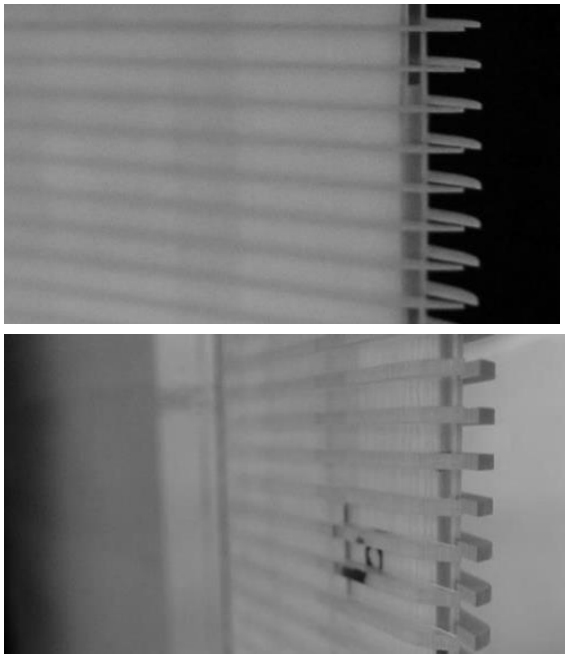

***Figure 20**. Comparison of configurations 5 (top) and 9 (bottom) illustrating the difference in fence thickness. Pictures are looking upstream from the trailing edge*

Assuming overall boundary layer thicknesses five to ten times these values, it is clear that increasing the fence height from 4 to 8mm would cause the fences to cut substantially more of the boundary layer, particularly on the suction side, and thus have a greater impact on the spanwise correlation lengthscale and thus the radiated noise. This conceptual model implies that further noise reductions at high angle of attack could be achieved by increasing the height of the suction side fences, in accordance with the increase in boundary layer thickness.

Unlike other configurations, the 8-mm high fence treatment of case 8 was tested twice, the second time with the drag rake system in place. Figure 18 compares the drag on the airfoil with this treatment, with that of the clean case

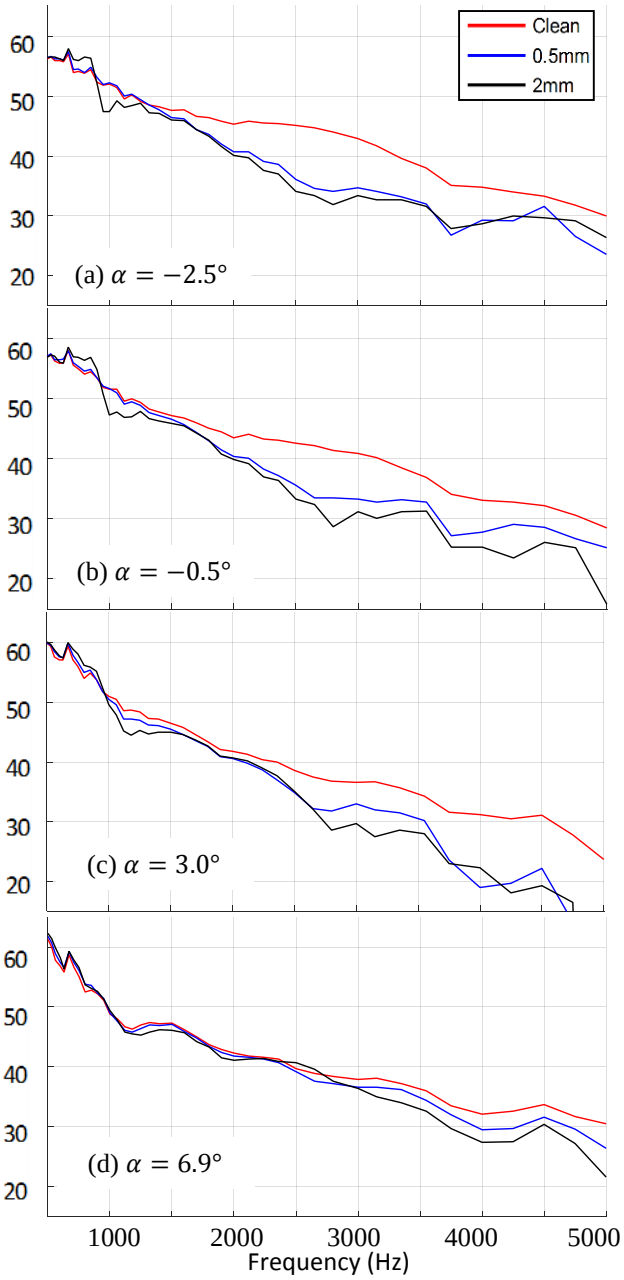

***Figure 21**. Noise spectra (in SPL re $20\,\mu Pa$) for configurations 5 and 9 contrasting the effects of fence thickness compared to the clean case. Re=3 million.*

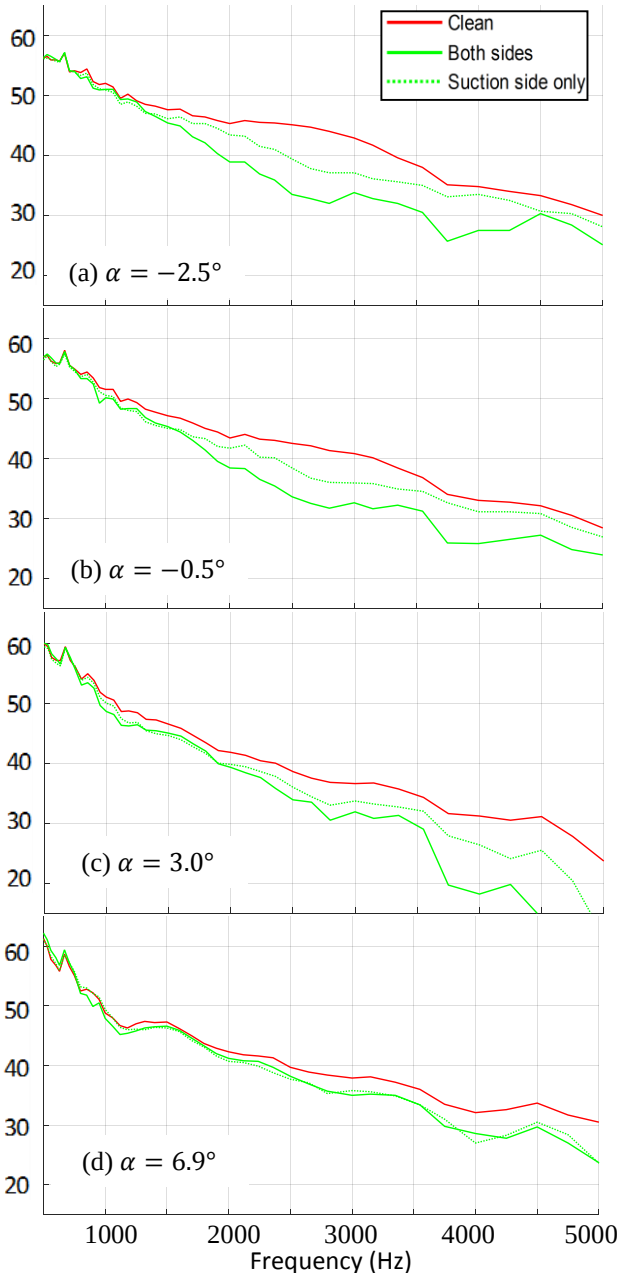

***Figure 22**. Noise spectra (in SPL re $20\,\mu Pa$) for configurations 8 and 8S contrasting the effects of applying the treatment to both sides of the airfoil (8) and just the suction side (8S), compared to the clean case. Re=3 million.*

and of the corresponding substrate alone case (configuration 2). The clean airfoil exhibits a drag bucket with a minimum C_d of about 0.008 near the zero-lift angle of attack of -2.5°. The drag then rises gradually with angle of attack through an angle of attack of 8° after which the airfoil stalls resulting in erratic fluctuations in the drag curve and overall a sudden rise. (Note that the slight reduction in C_d between 8° and 11° is a consequence of basing the drag on a wake measurement at a single spanwise station – three dimensional flow at the initiation of stall can result in a local thinning of the wake, despite its overall dramatic growth.) Adding the substrate to the airfoil (configuration 2) has no significant impact on the unstalled drag. Adding the 8-mm high fences of configuration 8 increases the drag by about 10%. Per 4mm of span, the airfoil has a surface area of some 6400 square millimeters. The fences add about 500 square millimeters to this total, or about 8%.

In other words, to the accuracy of its measurement, the increase in wetted surface area associated with the fences accounts for the drag increase.

Configuration 9 replicates the fence geometry of configuration 5, but with 2-mm thick in place of 0.5-mm thick fences and with a 0.75-mm thick substrate in place of a 0.5-mm thickness, figure 19. The effects of these changes on the sound heard above the suction side of the airfoil are shown in figure 20. Above 1.5kHz the effects of these geometry changes is a slight reduction (up to about 3dB) on acoustic levels. Some fraction of these could, perhaps, be ascribed to the substrate effect (figure 13), but at the very least we see that the thicker fences are not detrimental to the acoustic performance of the treatment. The results below 1.5kHz are less clear. At the lower angles of attack, acoustic levels appear suppressed by the thicker treatment around 1100Hz but increased by it at around 700Hz, perhaps indicating that the fences initiate some organized turbulent motion at these low frequencies.

Figure 21 shows the effects of only using the treatment on the suction side of the airfoil vs. both sides. In both cases the treatment is 8-mm high fences with a spacing of 8mm. At angles of attack of -2.5º, -0.5º and 3º the effect of removing the pressure side treatment is, to a good approximation, to halve the decibel attenuation produced by the treatment. It is hard to draw a solid quantitative inference from this since it is unclear how much of the sound is generated by the suction and pressure side boundary layers, and by the interaction between them. However, if we assume equal contributions from both boundary layers and no interaction effect, then a complete elimination of the sound from the suction side boundary layer would be observed as a broadband 3dB reduction relative to the clean airfoil. At 6.9 degrees angle of attack the removal of the pressure side treatment has no effect on the sound radiated from the foil. This suggests that either the pressure-side treatment is ineffective at large angles of attack or, as seems more probable, the suction-side boundary layer is the dominant contributor to the far-field sound at such conditions.

D. Effects of the rail treatments

Figure 23 shows the first rail case, configuration 14, installed on the trailing edge portion of the airfoil trailing edge region. This configuration uses 1.25-mm diameter rails rising to 4mm above the airfoil surface and spaced at 2.5-mm intervals across its span. The rails extend 10-mm downstream of the trailing edge. In terms of aerodynamic performance, all the rail cases produced lift curves almost indistinguishable from those of configuration 5, shown in figure 10. Drag measurements were not made with the rail cases.

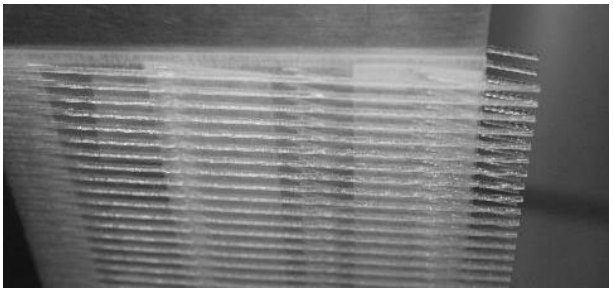

Figure 23*. Side view of configuration 14 applied to both sides of the airfoil showing the rail geometry*

The geometric parameters of configuration 14 do not exactly match any of the fence cases but fall somewhere between configuration 3 (4-mm high fences with 1mm spacing) and configuration 5 (4-mm high fences with 4mm spacing). Noise measurements made with configurations 14, 3 and 5 are compared with those for the clean airfoil in figure 24. At angles of attack of -2.5º,-0.5º, and 3º the rail treatment produces almost identical noise attenuation to the 4-mm spaced fences and, unlike the 1-mm spaced fences, there is no evidence of low frequency vortex shedding associated with an effective increased trailing edge thickness. Close to stall, however, at an angle of attack 6.9º the rails perform significantly better than the fences producing detectable attenuation at frequencies down to 2 kHz and doubling the dB attenuation at higher frequencies.

The acoustic performance of a selection of the other rail cases is plotted in figure 25. This includes elimination of the trailing edge extension (configuration 15), doubling of the maximum rail height to 8mm (configuration 17) and doubling of the diameter and spacing to 2.5mm and 8mm respectively (configuration 18). The change that has the least effect appears to be the elimination of the trailing edge extension which has no impact on the sound attenuation compared to configuration 14 other than, perhaps, a slight reduction in attenuation at the very highest frequencies. As with the fence configurations, increasing the spacing (config. 18), reduces the attenuation achieved by the treatment by a few dB above about 2500Hz. Contrary to what was seen with the fences, doubling the maximum height of the rails to 8mm (compare configurations 14 and 18) is actually counter-productive particularly at the highest angle of attack (6.9º) where the additional height might expect to be beneficial in penetrating the thicker suction side boundary layer. It may be that, if made too large, the space under the rails may permit re-connection of spanwise coherent structures and thus limit the reduction in spanwise correlation lengthscale that can be achieved.

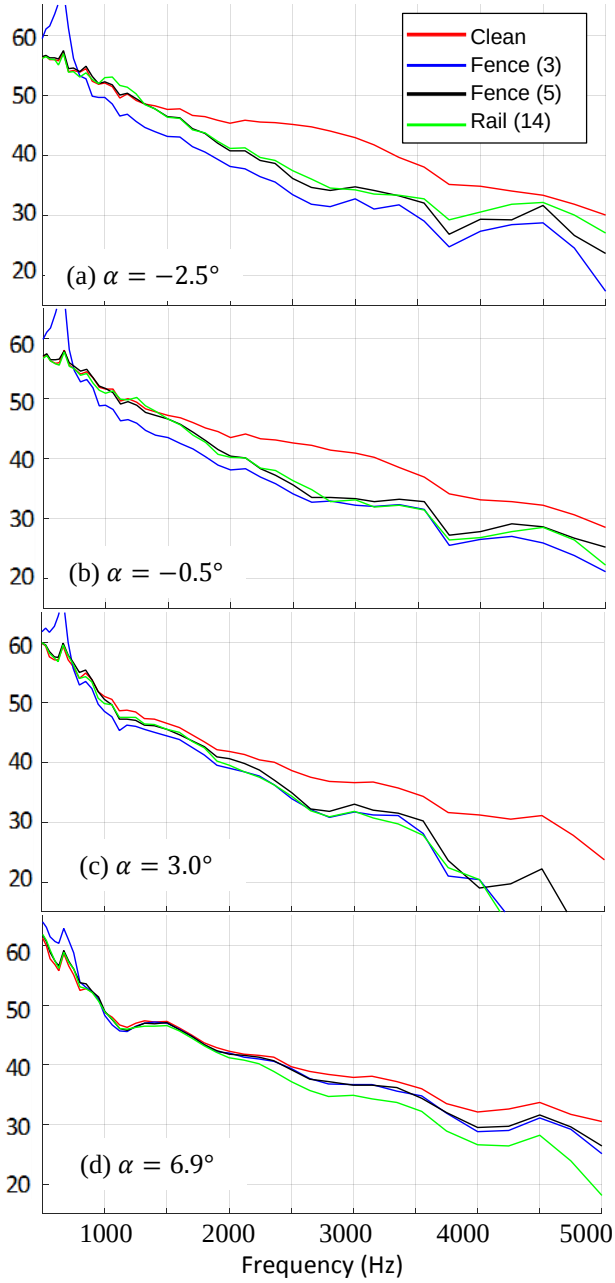

Figure 24. *Noise spectra (in SPL re 20 μPa) for configurations 3, 5 and 14 contrasting the effects of fence and rail treatments of similar scale, compared to the clean case. Re=3 million.*

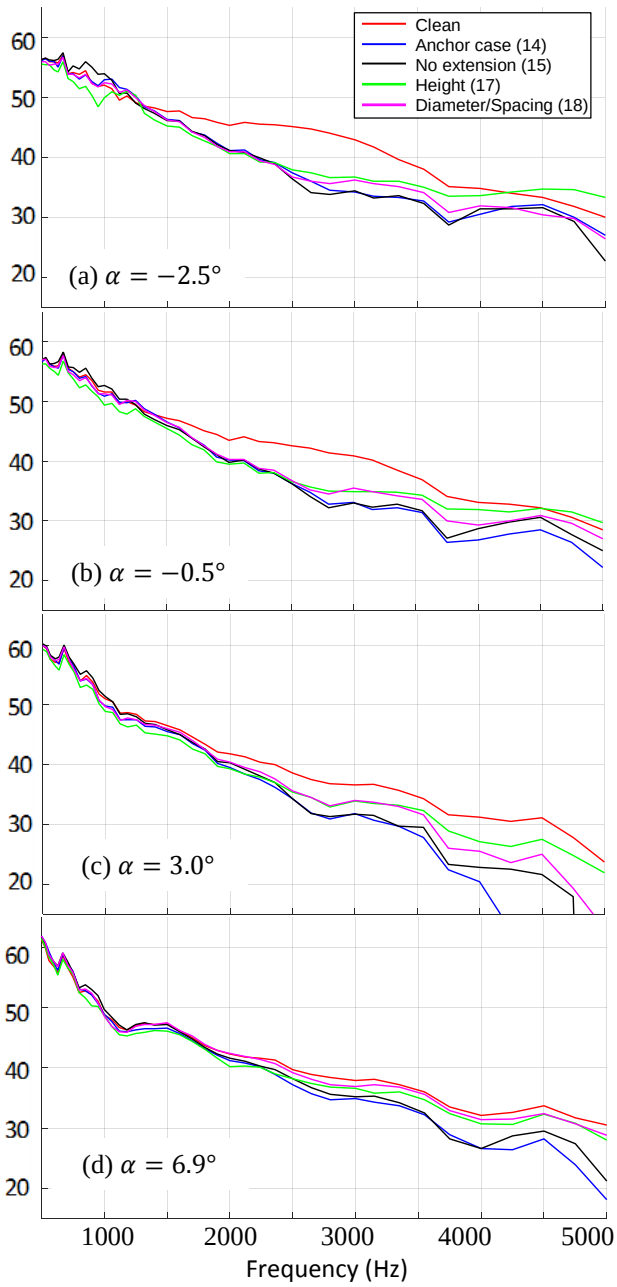

Figure 25. *Noise spectra (in SPL re 20 μPa) for configurations 14, 15, 17 and 18 contrasting the effects of different rail treatments, compared to the clean case. Re=3 million.*

IV. Conclusions

Airfoil treatments to reduce trailing edge noise, inspired by the downy canopy found to coat the flight feathers of some owls, have been developed. These treatments were designed to replicate the surface-pressure-attenuating effects of the canopy in a form suitable for application to an airfoil.

Over 20 variants of these designs have been tested by performing aeroacoustic wind tunnel measurements on a tripped DU96-W180 airfoil at chord Reynolds numbers up to 3 million. Variations include treatment thickness, density, length, position relative to the trailing edge and the effectiveness of treating only one side of the trailing edge. Compared to the untreated airfoil the treatments were found to be quite effective, providing broadband attenuation of trailing edge noise of up to 10dB.

The attenuation is found to be robust to changes in non-dimensional flow parameters, and there appears to be good potential for tailoring the treatment to suit engineering system design requirements. Treatments were found to be effective over an angle of attack range that extends over 9 degrees from zero lift. Airfoil treatments were observed to have no detrimental effect on the lift performance of the airfoil. Drag is slightly increased but only by an amount commensurate with the increase in wetted surface area associated with the treatment.

Acknowledgments

The authors would like to thank the Office of Naval Research, in particular Drs. Ki-Han Kim and Woei-Min Lin, for their support under grants N00014-13-1-0244, N00014-14-1-0242, and N62909-12-1-7116 (NICOP). The assistance of Prof. Aurelien Borgolz and Mr. Tim Meyers over the course of the wind tunnel testing, and the support of the College of Engineering at Virginia Tech in performing that testing, are gratefully acknowledged. Thanks also go to Mr. Daniel Grohol for his assistance in performing computer aided design of the trailing edge treatments, and Mr. Scott Patrick for his help with their manufacture.

The authors take particular pleasure in acknowledging Professor Geoffrey Lilley, whose long-standing interest in and insight into the aeroacoustics of the owl has been a source of great inspiration.

References

Alexander, W. N., Devenport, W. J., Clark I. A., Jaworski, J. W., Glegg, S., Peake, N. and Daly, C., 2014, "Noise Reduction Surface Treatment for Airfoil", International Patent Application PCT/US14/59508.

Choi, K., and Simpson, R.L., 1987, "Some Mean Velocity, Turbulence and Unsteadiness Characteristics of the VPI & SU Stability Wind Tunnel," Department of Aerospace and Ocean Engineering, Virginia Polytechnic Institute and State University, Blacksburg, Virginia 24061, Report VPI-Aero-161.

Clark, I. A., Devenport, W. J., Jaworski, J. W., Daly, C., Peake, N. and Glegg, S., 2014, "The Noise Generating and Suppressing Characteristics of Bio-Inspired Rough Surfaces", AIAA/CEAS 20th Aeroacoustics Conference, Atlanta, GA, 16-20th June. AIAA 2014-2911

Devenport, W. J., Burdisso, R. A., Borgoltz, A., Ravetta, P. A., Barone, M. F., Brown, K. A. and Morton, M. A., 2013, "The Kevlar-walled anechoic wind tunnel", *Journal of Sound and Vibration*, vol. 332(17), pp. 3971-3991.

Glegg, S. and W. Devenport, 2009, "The far-field sound from rough-wall boundary layers." *Proceedings of the Royal Society A: Mathematical, Physical and Engineering Sciences*, Vol. 465, pp. 1717-1734.

Graham, R. R., "The silent flight of owls," *J. R. Aero. Soc.*, Vol. 38, 1934, pp. 837-843.

Kroeger, R. A., Gruschka, H. D., and Helvey, T. C., 1972, "Low speed aerodynamics for ultra-quiet flight," *Tech. Rep.* AFFDL-TR-71-75, Air Force Flight Dynamics Laboratory, Wright-Patterson AFB.

Jaworski, J. W. and Peake, N., 2013a, "Aerodynamic noise from a poroelastic edge with implications for the silent flight of owls," *J. Fluid Mech.*, Vol. 723, pp. 456-479.

Jaworski, J. W. and Peake, N., 2013b, "Parametric guidance for turbulent noise reduction from poroelastic trailing edges and owls," *Proceedings of the19th AIAA/CEAS Aeroacoustics Conference*, Berlin, AIAA-2013-2007.